

---

# SPATIO-TEMPORAL SMALL AREA SURVEILLANCE OF THE COVID-19 PANDEMICS

---

A PREPRINT

**Miguel A. Martínez-Beneito**

Department of Statistics and Operations Research.  
University of Valencia.  
Burjassot (Valencia).  
miguel.a.martinez@uv.es

**Jorge Mateu**

Department of Mathematics  
University Jaume I of Castellon  
Castelló de la Plana  
mateu@uji.es

**Paloma Botella-Rocamora**

Subdirecció General d'Epidemiologia, Vigilància de la Salut i Sanitat Ambiental.  
Conselleria de Sanitat Universal i Salut Pública. Generalitat Valenciana.  
Valencia.  
botella\_pal@gva.es

November 10, 2020

## ABSTRACT

The emergence of Covid-19 requires new effective tools for epidemiological surveillance. Spatio-temporal disease mapping models, which allow dealing with highly disaggregated spatial and temporal units of analysis, are a priority in this sense. Spatio-temporal models provide a geographically detailed and temporally updated overview of the current state of the pandemics, making public health interventions to be more effective. Moreover, the use of spatio-temporal disease mapping models in the new Covid-19 epidemic context, facilitates estimating newly demanded epidemiological indicators, such as the instantaneous reproduction number  $R_t$ , even for small areas. This, in turn, allows to adapt traditional disease mapping models to these new circumstances and make their results more useful in this particular context. In this paper we propose a new spatio-temporal disease mapping model, particularly suited to Covid-19 surveillance. As an additional result, we derive instantaneous reproduction number estimates for small areas, enabling monitoring this parameter with a high spatial disaggregation. We illustrate the use of our proposal with the separate study of the disease pandemics in two Spanish regions. As a result, we illustrate how touristic flows could have shaped the spatial distribution of the disease. In these real studies, we also propose new surveillance tools that can be used by regional public health services to make a more efficient use of their resources.

**Keywords** Covid-19 · disease mapping · instantaneous reproduction number · spatio-temporal modeling

## 1 Introduction

Covid-19 has emerged as a novel health problem, posing new challenges and pressure to health systems, in particular public health services. As a consequence, new tools and research are required in order to solve the problems arising from this pandemic. On one hand, biomedical research is required in order to either develop new vaccines that could stop, or at least decrease, the spread of the disease or new treatments that could help to handle the disease in clinic terms. On the other hand, new public health methodologies and tools are also required in order to address the corresponding health threaten that affects population worldwide. Indeed, it has been recently stated that “countries should not ease restrictions until they have robust systems in place to closely monitor the infection situation” (Han et al. 2020). In this context, the development of effective epidemiological surveillance tools that could make it possible to focus public

health efforts on particular locations and moments are a high priority. These tools would be a valuable help in the current setting, where the public health resources demanded by the pandemic are frequently higher than those available; thus, having a precise guidance on where and when actions should be taken to control the pandemic is crucial.

A compulsory requirement of effective epidemiological surveillance systems is dealing with sufficiently disaggregated data, both in space and time. Surveillance systems working with either large spatial units or long time units will be neither specific nor updated enough as to provide useful results in epidemiological terms. Anyway, handling highly disaggregated data in terms of either space or time poses statistical challenges, known in the statistical literature as small areas estimation problems (Rao 2003), that should be solved if results with sufficient reliance are really wanted. In this sense, the small area and disease mapping literature (Lawson 2018; Martinez-Beneito and Botella-Rocamora 2019) could be useful for this purpose, and the use of spatio-temporal disease mapping models could be of particular interest.

Most epidemiological surveillance systems use incidence rates as main indicator of the current state of any disease outbreak. A vast literature exists on the small areas smoothing of rates, in particular standardised rates, which allow visualising current incidence levels, even dealing with highly disaggregated areal data (Besag, York, and Mollié 1991; Leroux, Lei, and Breslow 1999). Nevertheless, Covid-19 pandemic has focused substantial attention also on the instantaneous reproduction number  $R_t$  (Nishiura and Chowell 2009), but no small areas estimation literature is available for this indicator. For each time period  $t$ ,  $R_t$  can be interpreted as the basic reproduction number of the disease,  $R_0$  (Milligan and Barrett 2014), corresponding to that particular time period. Thus,  $R_t$  could be interpreted as a temporally dynamic version of  $R_0$ . The basic reproduction number  $R_0$  is defined as the number of people that would be infected, in average, in a completely susceptible population by a single infected person. For  $R_0 > 1$  the pandemic has an explosive increasing evolution while for  $R_0 < 1$  it tends to fade out in a given period of time. As made clear in this Covid-19 pandemic, where mitigation actions have been undertaken at different time moments, there is no a single static value for  $R_0$  inherent to the disease (Wilasang et al. 2020; Fang, Nie, and Penny 2020). On the contrary,  $R_t$  shows substantial temporal variability and this statistic is an interesting quantity that allows monitoring the rate of spread of the disease at every single moment of the period of study, addressing if the epidemiological control measures undertaken are enough, or not, to stop the spread of the disease. While temporal variability of  $R_t$  is frequently assessed by surveillance systems, the geographical variability of this indicator is usually unknown, at least with a sufficiently high disaggregation level. This avoids that specific epidemiological measures are taken wherever they are required according to this criterion.

Estimating  $R_t$  can be problematic in some particular settings. For example, the scarce daily information on the observed counts analysed by Cori et al. (2013) made them to consider weekly temporal units of analysis, where the cases observed during the week before day  $t$  were gathered in order to estimate  $R_t$  on that precise day. As a consequence, they considered consecutive overlapping time windows for their analysis (one for each  $R_t$ ), ignoring the dependence that this could yield on the data. Ignoring such dependence could have an impact on some issues, as for example the width of confidence intervals for the different  $R_t$ 's. Moreover, the weekly character of those time windows makes the observed cases of the disease to be averaged during the last observed week, making  $R_t$  less sensible to the latest incidence changes that the time series could show. This makes the interest of  $R_t$  decrease as an epidemiological surveillance tool. This modelling approach is implemented in the `EpiEstim` (Cori 2020) R package, which is being extensively used for many public health institutions for Covid-19 surveillance tasks (see Tebé et al. (2020) or Centro Nacional de Epidemiología. Instituto de Salud Carlos III (2020) for just two examples).

The statistical problems of  $R_t$  estimation just mentioned are mainly due to the few observed cases available per time unit when the units of analysis are small. However, these problems would be exacerbated if several spatial units of study were considered, instead of a single unit, since those units would split the observed daily cases into smaller quantities. In that case, a small areas modelling framework would be required in order to yield sensible incidence estimates sharing information between neighbouring sites, since otherwise those estimates would mainly reproduce the high amount of noise that such small figures frequently show.

In this paper we propose a small areas spatio-temporal model specifically devised for Covid-19 incidence data. With our proposal we seek to develop advanced surveillance tools that allow monitoring the disease at high disaggregation levels. In real terms, this would make it possible to implement specific epidemiological control measures wherever and when they are required according to detailed and specific information. Additionally, our spatio-temporal model also allows to visualize the temporal evolution of the geographical pattern of the disease. Visualising that evolution helps understanding the performance of the disease and shows how the different control measures implemented throughout the period of study have modified that spatial distribution.

In addition, we apply the spatio-temporal model developed in this paper to two real Covid-19 data sets. These data sets correspond to surveillance data of two Spanish regions with a high spatial and temporal disaggregation. Specifically, these data sets contain the daily observed incident cases for a detailed division of both regions, with less than 10000 people in average per spatial units in both cases, and with substantially lower population in many particular cases. The application of our model to these data sets illustrate its impact in practical terms.

This paper is organised as follows. Section 2 introduces a general spatio-temporal modelling proposal for the analysis of Covid-19 surveillance data sets of potential use in many different regions. Section 3 shows the application of that model to the analysis of the Covid-19 pandemics in two Spanish regions. This section illustrates the real use in practice of our strategy and the corresponding results. Finally, Section 4 discusses some aspects of the model introduced and its use for Covid-19 surveillance.

## 2 Modelling proposal

We consider the following general setting that, in principle, could be easily adapted or directly used for many small areas Covid-19 surveillance studies. Let us assume that we have a region of study divided into  $I$  spatial units, of small size in a statistical sense, observed during  $J$  consecutive days. Let  $O_{ij}$  denote the observed number of incident Covid-19 cases for the  $i$ -th spatial unit ( $i = 1, \dots, I$ ) and the  $j$ -th day ( $j = 1, \dots, J$ ) of the period of study. We consider the observed cases to be independently Poisson distributed, given the underlying process  $\lambda$ , as  $O_{ij} \sim \text{Poisson}(\lambda_{ij})$ , and model the underlying process as

$$\log(\lambda_{ij}) = \log(P_i) + \gamma_{DoW(j)} + (\beta\mathbf{X})_{ij} + \epsilon_{ij}$$

where:

- $P_i$  is the population living at the  $i$ -th spatial unit during the period of study. This quantity is considered constant in time during all that period.
- $\gamma$  is a vector, of length 7, intended to model the supposedly important cyclic effect of the different week days on the incidence rates. The term  $DoW(j)$  denotes a function that returns the day of the week, as a value between 1 and 7 corresponding to the  $j$ -th day of the period of study.
- $\mathbf{X}$  is a  $K \times J$  design matrix, where each column corresponds to a different day and each row corresponds to a different basis function, intended to model the incidence rates time trend for the different spatial units.  $X_{kj}$  stands for the value of the  $k$ -th basis function on the  $j$ -th day. This matrix is fixed by design and no inference is made on  $\mathbf{X}$ .
- $\beta$  is an  $I \times K$  matrix with the coefficients of the basis functions used for modelling the incidence rate time trend for each spatial unit. The variability of the different rows of  $\beta$  allow the incidence rates of the spatial units to follow different trajectories.
- $\epsilon$  is an  $I \times J$  matrix of independent random effects. This unstructured term is intended to model the overdispersion of the Poisson process beyond the variability induced by the rest of terms in the model. Covid-19 incident cases tend to cluster in some particular days for each spatial unit due to either the outbreak nature of these cases that makes them to be grouped, or some other artifacts, such as the sampling of several suspicious cases around the first index case of an outbreak, which will usually be all tested in a same day. These artifacts may produce abnormally high numbers of cases for some particular days and locations, beyond the smooth time trend of the disease, that we try to take into account with this term.

The spatio-temporal variability of the process is mainly modelled by the product  $\beta\mathbf{X}$ . This product relies on an appropriate basis of functions suitable for modelling the temporal variability of the disease. Once these functions are chosen, the coefficients  $\beta$  combine them in order to define the time trends for the disease; a different time trend for each spatial unit. Moreover, the number of functions in the basis  $K$  may be different to the number of days  $J$  in the period of study, in particular it could be substantially lower. This makes the time trend for each spatial unit depend on just a few parameters  $K$ , much lower than the number of observations on that spatial unit  $J$ , making a low-dimensional fit of that time trend, quite convenient in computational terms.

Although we could formulate the model above for a general basis of functions  $\mathbf{X}$ , we find it particularly convenient the use of splines as basis of functions for modelling the temporal variability of the incidence rates. In particular, we propose to use a basis of natural cubic B-splines for that goal. Besides its computational convenience, B-splines have the advantage of having compact support, thus the elements of this basis model the temporally local performance of the incidence curve during an interval of days, making the interpretation of the corresponding coefficients  $\beta$  quite straightforward. Moreover, the use of natural splines makes the fit of the incidence trends to be particularly sensible at the extremes of the period of study, specifically at the end of that period. This is particularly convenient for surveillance purposes, where attention is usually put on these precise days of the period of study.

Our proposal models the incidence time trends by means of the fitted splines. On the other hand the spatial smoothing of the incidence rates is carried out through the matrix of spline coefficients  $\beta$ , in particular the spatial dependence of its cells. Specifically, we model those cells as  $\beta_{ik} = \mu_k + \beta_{ik}^*$ , where  $\mu_k$  models the mean value, across the set of spatial units, of the coefficient corresponding to the  $k$ -th spline in the basis. These values will change according to the mean

incidence level at each moment of the period of study, and the vector  $\boldsymbol{\mu} = (\mu_1, \dots, \mu_K)$  accounts for those overall temporal variations. On the other hand, the matrix  $\boldsymbol{\beta}^*$  models the spatial variability of the different incidence time trends. This term allows each spatial unit to follow a different time trend. For inducing a smooth spatial performance, we model the columns of this matrix as spatial random effects following some Gaussian Markov random field (Rue and Held 2005). In this sense we could use for example a proper CAR distribution, a combination of an Intrinsic CAR and an heterogeneous random effect, as proposed by Besag, York, and Mollié (1991) or the CAR distribution of Leroux, Lei, and Breslow (1999). In our case we opt by using the latter option for inducing spatial dependence on the incidence rates, i.e., we assume the following set of conditional distributions

$$\beta_{ik}^* \sim N \left( \frac{\rho_k}{1 - \rho_k + \rho_k n_i} \sum_{i' \sim i} \beta_{i'k}^*, \frac{(\sigma_\beta^2)_k}{1 - \rho_k + \rho_k n_i} \right).$$

where the subindex  $i' \sim i$  denotes all spatial units  $i'$  adjacent to spatial unit  $i$  and  $n_i$  denotes the number of neighbours of that area. In these conditional distributions  $\rho_k$  takes values in the interval  $[0, 1]$ , and this parameter may reproduce either an heterogeneous process for  $\rho_k = 0$ , an intrinsic CAR distribution for  $\rho_k = 1$  or intermediate process, with stronger or weaker spatial dependence, for  $\rho_k \in ]0, 1[$ . Considering different  $\rho_k$  and  $(\sigma_\beta^2)_k$  parameters for each element in the basis of functions allows reproducing different spatial strengths and different spatial variabilities, respectively, for the different moments of the period of study. As a consequence, this reproduces a non-separable spatio-temporal correlation structure (Torres-Avilés and Martínez-Beneito 2015). These assumptions seem reasonable when the pandemic could show very different spatial features at the different phases of the pandemic waves or even at the different waves of the pandemic.

The term  $\boldsymbol{\beta X}$  in the linear predictor models, for each spatial unit, the temporal variability of the Covid-19 incidence along the period of study. On the other hand, the term  $\boldsymbol{\gamma}$  is in charge of modelling the cyclic variability within weeks. This term is mainly required to take into account the different incidence rates that weekends could have in comparison to weekdays. We will consider the *DoW* function to be equal to 1 for the first day of study and it will increase, day by day, until 7. Afterwards, *DoW* will reproduce this cycle repeatedly. The first element of the vector  $\boldsymbol{\gamma}$ ,  $\gamma_1$ , will be fixed to 0 and therefore the rest of elements of  $\boldsymbol{\gamma}$  will model the departures of the incidence rates of the rest of week days, in comparison to the first. Improper uniform prior distributions on the whole real line are assigned to  $\gamma_2, \dots, \gamma_7$ .

Finally, regarding the cells of the matrix of random effects  $\boldsymbol{\epsilon}$ , they are modelled as independent  $N(0, \sigma_\epsilon^2)$  variables. In this case,  $\sigma_\epsilon^2$  is also estimated within the model and a *Uniform*(0,  $c$ ) distribution, for a large enough (non informative) value  $c$ , is assigned to the standard deviation  $\sigma_\epsilon$ .

## 2.1 Small areas estimation of the instantaneous reproduction number $R_t$

One advantage of our proposal for spatio-temporal modelling of the COVID-19 incidence, is that we could provide small areas estimates of some epidemiological quantities of particular interest, such as the instantaneous reproduction number  $R_t$  for all days  $t$  of the period of study, and for the small areas division of the region of study. Specifically, we will estimate  $R_{it}$ , the instantaneous reproduction number for each (small) spatial unit  $i$  and each day  $t$  of the period of study.

In a non-spatial setting, leaving aside the influence of the prior distribution used for the different  $R_t$ 's, the widely used *EpiEstim* package of R estimates the  $R_t$ 's as  $O_t / (\sum_{s=1}^S O_{t-s} w_s)$ , where  $O_t$  denotes the incident cases for the whole region at the  $t$ -th day of study. In this expression  $w_s$  denotes the *infectivity function* that quantifies, for each lag time  $s$ , the probability of observing an  $s$ -days difference between two cases, one primary and one secondary case of the disease, being  $S$  an upper bound for the subindex  $s$ . The incident cases  $O_t$  could be quite low for some days of the period of analysis, even for the whole region of study, what could make  $R_t$  to be noisy and unreliable. As a potential solution, these authors propose to use overlapping time windows of size  $\tau$  instead of single days and therefore estimate  $R_t$  instead as

$$\left( \sum_{k=t-\tau+1}^t O_k \right) / \left( \sum_{k=t-\tau+1}^t \sum_{s=1}^S O_{k-s} w_s \right).$$

This illustrates how the  $R_t$  estimation poses particular problems, mainly when small counts are frequent. This will be the usual case when working with small sized spatial units, justifying the use of particularly suited methods if these indicators were to be calculated on that particular setting. According to the disease mapping literature, if  $O_i \sim \text{Poisson}(\lambda_i)$  are the observed counts of some disease at the  $i$ -th spatial unit, and  $E_i$  the corresponding expected counts, the Standardised Incidence Ratio (SIR) for that spatial unit is defined as  $SIR_i = O_i / E_i$ . This risk estimate shows similar small areas problems to those just introduced, arising from the small values that  $O_i$  and  $E_i$  usually take. These problems are normally solved by considering an smoothed version of those SIRs defined as  $SIR_i = \lambda_i / E_i$ , where

$\lambda_i$  is estimated taking into account the incident cases of that spatial unit and the underlying hypotheses of the model, that will usually induce spatial dependence on  $\lambda_i$ . We follow a similar approach for deriving smoothed instantaneous reproduction numbers that could solve the small areas problems of the corresponding unsmoothed indicator.

In parallel to Cori et al. (2013), and following the disease mapping smoothing ideas just mentioned, we could estimate  $R_{it}$  for the small area  $i$  and day  $t(= S + 1, \dots, J)$  as:  $R_{it} = \lambda_{it} / (\sum_{s=1}^S \lambda_{i,t-s} w_s)$ , where  $\lambda_{it}$  is now the expected incident cases for that spatial unit and day according to our model. We could set  $\lambda_{it}$  to be equal to  $\exp(\log(P_i) + \gamma_{DOW(t)} + (\beta\mathbf{X})_{it} + \epsilon_{it})$ , or simply  $\lambda_{it} = \exp(\gamma_{DOW(t)} + (\beta\mathbf{X})_{it} + \epsilon_{it})$  since the population term will cancel out in the numerator and denominator of  $R_{it}$ . Nevertheless, we could also remove the cyclic term in the latest expression, that is  $\lambda_{it} = \exp((\beta\mathbf{X})_{it} + \epsilon_{it})$  since, in this manner, we will filter out the cyclic effect that we could find in  $R_{it}$  as a consequence of that same artifact on the raw incidence figures and that we will not be typically interested in. Moreover, if  $\lambda_{it}$  was simply defined as  $\exp((\beta\mathbf{X})_{it})$ , we would obtain a parsimonious version of  $R_{it}$  where the particular data collecting features that could be having an influence on  $O_{it}$  are filtered out and just the smooth spatio-temporal trend captured by the spline process would be kept. Thus, a parsimonious smoothed instantaneous reproduction number  $R_{it}$  suitable for small areas could be obtained as

$$R_{it} = (\exp((\beta\mathbf{X})_{it})) / \left( \sum_{s=1}^S \exp((\beta\mathbf{X})_{i,t-s}) w_s \right).$$

In the case that MCMC inference were performed on the model above, this would allow to calculate the different smoothed  $R_{it}$ 's at every step of the MCMC. This would allow to easily draw confidence bands for the smoothed instantaneous reproduction number for every spatial unit  $i$ . This, in turn, enables to easily draw  $P(R_{it} > 1)$  could be also calculated for each  $i$  and  $t$ , and therefore we can assess the probability of the epidemic to be out of control at every location and time of the period of study. This quantity, obviously, could be of evident interest for epidemiologists.

### 3 Spatio-temporal modelling of Covid-19 for two Spanish regions

We now study the Covid-19 pandemics in Spain, in particular in Castilla y Leon (CyL) and Comunidad Valenciana (CV), 2 out of the 17 Spanish communities, with 2.3 and 5 million inhabitants, respectively.

The CyL Covid-19 data are publicly available from <https:// analisis.datosabiertos.jcyl.es/pages/coronavirus/>. The period of study for this region covers the interval from March 6th to October 14th, 2020, which is the period publicly available at that webpage at October 18th, 2020, the day when this analysis was performed. Covid-19 data for CyL are published at the health zone level, an administrative division corresponding to the geographic units covered by the primary care centers of this region. CyL is divided into 247 health zones, with population ranging from 441 to 37509 inhabitants. The data set analysed contains daily observed Covid-19 counts for each of the CyL health zones. The data set used for this analysis is supplied as supplementary material to the paper in order to make this part of the analysis completely reproducible. This data set and the rest of supplementary material may be found at the webpage: <https://www.uv.es/mamtnez/ETCovid.html>.

CV data have been supplied, under request, by the Health Administration of this region. As for CyL, the data set contains daily observed Covid-19 counts for the 542 municipalities that form this region. Municipalities in CV are towns, in administrative terms, whose populations range from 17 to 794288 inhabitants in 2019. The median population per municipality is 1412 inhabitants. In this case the period of study covers once again the interval from March 6th to October 14th. The data for this analysis are not supplied since they are not publicly available.

MCMC Inference was carried out by using WinBUGS. Additionally, the pbugs R package (Vergara-Hernández and Martínez-Beneito 2020) was used for running in parallel the 5 MCMC chains simulated. 2000 MCMC draws were firstly simulated as burn in period of a total of 5000 draws per chain. Finally, 1 out of each 15 draws were saved yielding therefore a posterior sample of 1000 draws. Convergence was assessed by means of the Brooks-Gelman-Rubin statistic and the number of effective simulations (Gelman et al. 2014), which are directly provided by the pbugs package. Full details on the implementation of the model, and the rest of results/figures shown below, can be found at the Rmarkdown and pdf documents in the supplementary material, which contain the full code used to run this analysis.

For the long range time trend modelling, we chose a natural B-spline basis with one node every 2 weeks and 2 final nodes at the borders of the period of study. Thus, for a total of 223 days of study, the final basis contained 17 spline functions scattered around all the period of study, one spline function every 2 weeks. These 17 functions yielded enough flexibility for modelling the temporal evolution of rates and  $R_t$ 's, and reduced the computational burden of the model in comparison to a weekly basis which contained 33 spline functions, and therefore 33 spatial processes

to be estimated within the model. Regarding the infectivity function  $w_s$ , required for calculating the instantaneous reproduction numbers, we assume a shifted Gamma distribution of mean 4.7 and standard deviation 2.9. These values have been estimated for COVID-19 incidence by Nishiura, Linton, and Akhmetzhanov (2020). Additionally, we have fixed the maximum temporal lag for calculating  $R_t$  to  $S = 25$  since for the mentioned parameters for  $w_s$  we have  $\sum_{i=1}^{25} w_s > 0.9999$ , that is, COVID-19 cases are hardly contagious after those 25 days.

We have run the spatio-temporal model above for these two data sets, separately. In both occasions we have considered a single spatial parameter  $\rho$  instead of different parameters  $\rho_k$  for each element in the basis since we have not found evidence of needing different spatial parameters. Specifically, we run an additional model with different  $\rho_k$ 's per basis function and the posterior confidence intervals of these parameters substantially overlapped. In our model, with a common  $\rho$ , we obtained a posterior mean for  $\rho$  of 0.51 (95% credible interval: [0.43,0.60]) for CyL, while for CV that posterior mean was 0.45 (95% credible interval [0.36,0.57]), so in both cases the spatial dependence found was moderate. In contrast, we found evidence of needing different variance parameters for the spatial processes corresponding to each of the basis functions. This different variances allow the spatial distribution of the disease to show varying variability at different moments of the period of study. Thus, considering different  $\sigma_k$ 's allows the spatio-temporal process to be temporally heteroscedastic. Specifically, for CyL the spatial standard deviations for the coefficients of the splines basis range from 0.88 (95% credible interval [0.65,1.14]) to 2.14 ([1.76,2.56]), while for CV they range from 1.26 ([0,1.93]) to 3.29 ([2.76,3.90]).

Regarding the overdispersion term  $\epsilon$ , its standard deviation has a posterior mean of 0.56 (95% credible interval [0.55,0.57]) for CyL and of 0.77 ([0.75,0.79]) for CV. This shows how the sampling artifacts, which make incident cases to cluster in some particular days and locations, are stronger in CV than for CyL. Regarding the cyclic weekly term  $\gamma$ , we have found a difference of 0.94 units between the day with higher and lower incidence for CyL, and of 1.16 in CV. The 95% credible intervals for both days, for both regions, were clearly disjoint and distant, pointing out the need of this term within the model.

Figure 1 shows several results of the spatio-temporal model for both regions. The upper row of Figure 1 shows, for both regions, the fitted mean to the daily observed cases, with the corresponding 95% credible bands. We first note the very different scales for both regions, even though the CyL population is lower than half the CV population. The blue line in these plots corresponds to the time trends taking into account both the long range time trend (splines) and cyclic weekly terms. The effect of the cyclic term is evident. On the other hand, the black line reproduces just the time trend corresponding to the splines component of the fit. These curves filter out the cyclic pattern that in general we will not be interested in to reproduce in the pandemics surveillance. Both splines curves seem to perfectly capture the time evolution of the disease, filtering the artifacts that could make the observed cases for one particular day to deviate below or above that trend. From now on, the rest of results shown will be based only in the splines component of the time trend in order to filter out the cyclic effect that we will typically want to remove.

The bottom left plot of Figure 1 shows the daily evolution of the instantaneous reproduction number of the pandemics for both regions. This plot shows the overall time trends, for the whole regions, and their corresponding 95% credible bands. Note the effect of the different amount of observed cases for each region which makes the bands for CV to be substantially wider than for CyL. The daily  $R_t$ 's in this plot have been calculated by following the methodology described in the previous section for each municipality and averaging all those  $R_t$ 's throughout the whole region. These averages are weighted according to the different populations of the different spatial units. These curves have a high epidemiological value since they allow to know if the pandemics is either increasing ( $R_t > 1$ ) or decreasing ( $R_t < 1$ ) at any moment of the period of study. Moreover, if wanted, we may also easily assess the probability of any of these two states. These curves show some evident differences in the pandemics diffusion for both regions, as for example the different starting times of the second wave of the pandemics, which started way sooner for CV than for CyL.

The bottom right plot of Figure 1 shows the rates (per 100000 people) time trends for 4 CV municipalities. Rates, in contrast to the fitted observed cases, allow comparisons between regions regardless of their population sizes. These municipalities correspond to Valencia and Alicante, the two most populated cities in CV and placed 166 kilometers away. Additionally, we show also the rates for Massalfassar and Aigues, the two least populated neighbouring municipalities of Valencia and Alicante, respectively. As we see in Figure 1, the rates curve for Massalfassar resembles that of Valencia, in a similar manner to Aigues and Alicante since, for example, they show concurrent peak epidemics. This is a consequence of the spatial dependence of the Leroux et al.'s processes in our model. Anyway, although these curves are similar, we can see evident departures within both Massalfassar-Valencia and Aigues-Alicante. For example, the first wave in Aigues showed far lower rates than for Alicante besides these two cities are neighbours and one of them has a population more than 300 times higher than the other, what could make the Alicante time trend to completely determine that of Aigues. Something similar happens for the second wave of Valencia and Massalfassar.

Figure 2 shows, once again for Valencia, Alicante, Massalfassar and Aigues, the fitted mean to the daily observed cases (left-hand-side of the figure), with the corresponding 95% credible bands. The right-hand-side of this figure shows

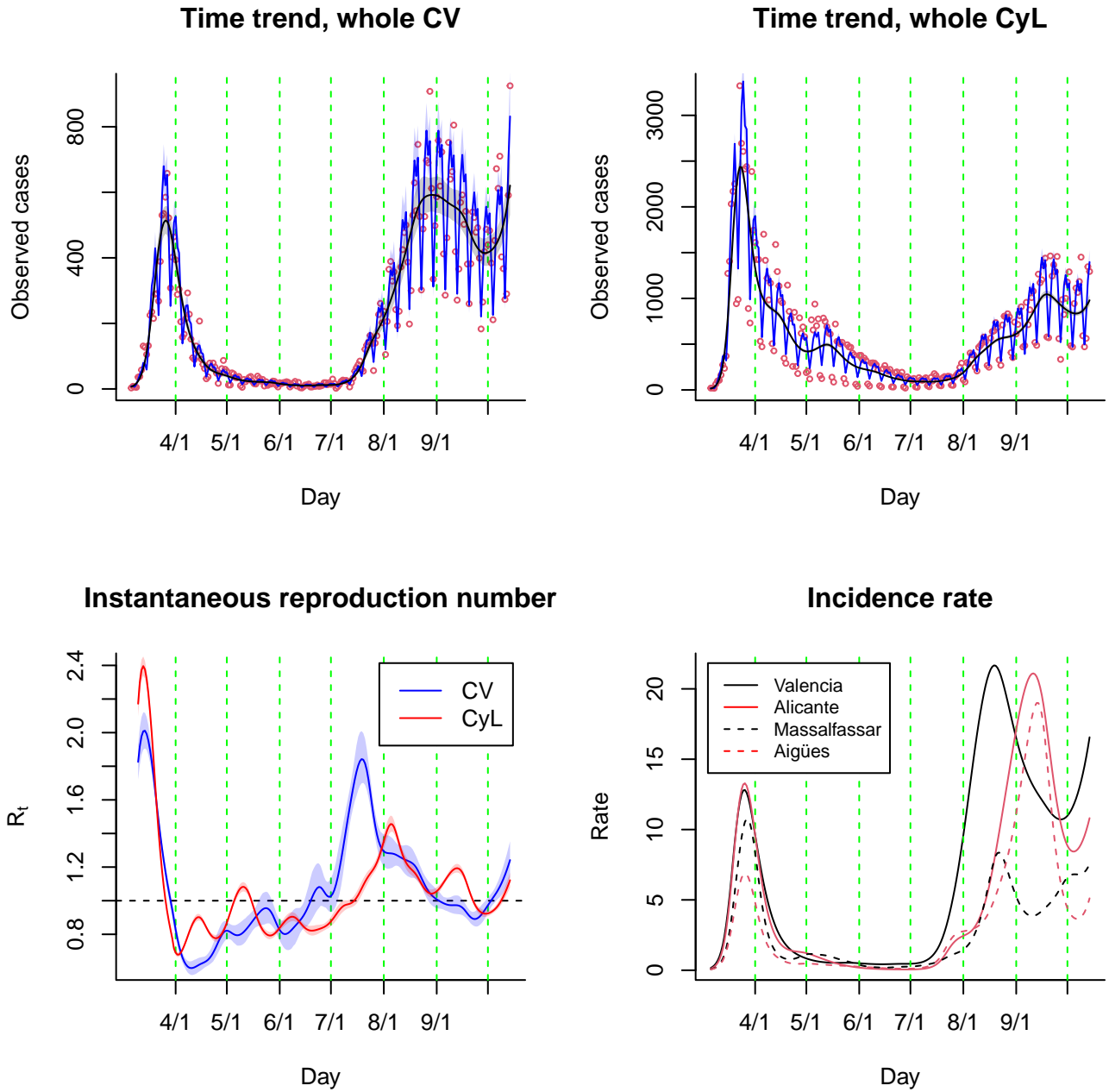


Figure 1: Overall time trends for the observed daily cases for both regions (top row). Estimated  $R_t$  evolution for both regions (bottom left plot), and daily rates per 100000 inhabitants for 4 municipalities in CV (bottom right plot).

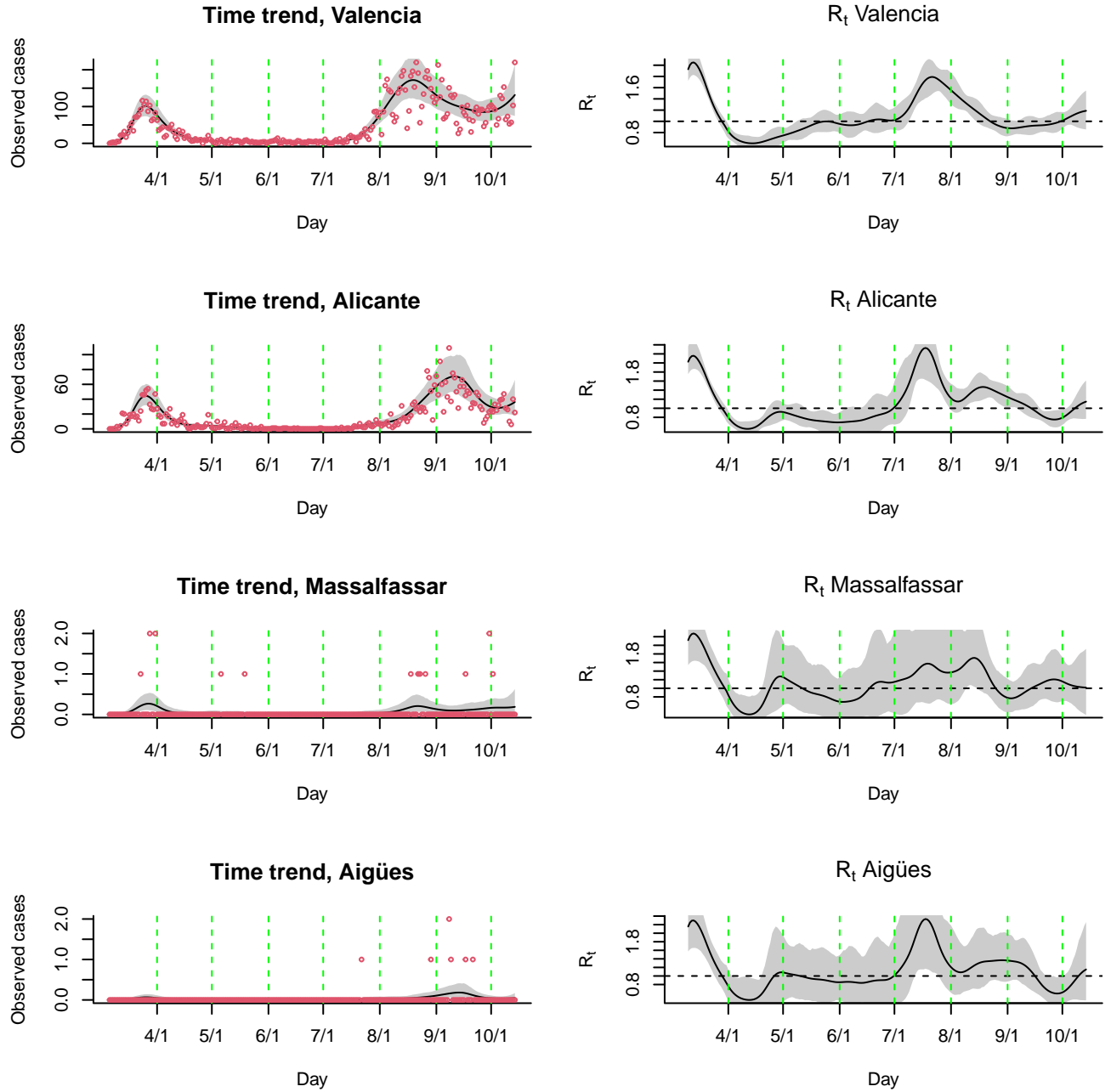


Figure 2: Observed daily cases time trend for Valencia, Alicante, Massalfassar and Aigües (left column), and  $R_t$  time trend for these same municipalities (right column).



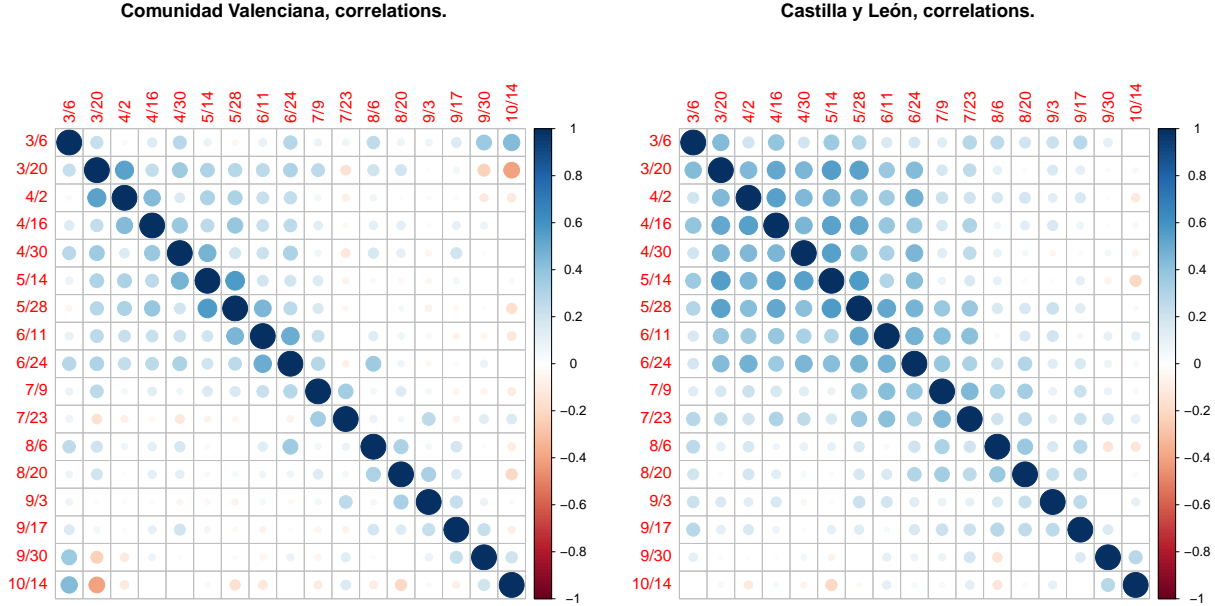


Figure 3: Correlation plots for the coefficients of the spline basis functions. Names of the rows and columns of the plot correspond to the day showing the peak of the corresponding spline function.

the  $R_t$  temporal evolution for each of these municipalities. The plots of the observed cases for Valencia and Alicante show a good fit, thus the biweekly splines used seem enough for describing the temporal variability of the observed cases in these large cities. On the other hand, for Massalfassar and Aigues, the observed cases are quite low due to the small size of these municipalities. Nevertheless, a time trend is fitted also for these municipalities which merges the information on the observed cases of these municipalities and the information provided by their neighbours. Thus, the time trend for Massalfassar resembles that of Valencia, with a long right tail at the second wave of the pandemic; larger than that of Aigues which resembles more the time trend for Alicante. Interestingly, Aigues does not have any observed case at the first wave of the pandemics, what explains the discrepancy between Alicante and Aigues at the first wave of the pandemics already shown in Figure 1.

Regarding the temporal evolution of the  $R_t$ 's for these municipalities, it is remarkable the longer width of the Massalfassar and Aigues 95% credible intervals for  $R_t$  in comparison to those of Valencia and Alicante. For example, it is rare to find some day during the second wave of the pandemic in Massalfassar and Aigues where the corresponding credible interval does not contain the value 1. On the contrary, for Valencia and Alicante most of the months of July and August showed  $R_t$  values significantly higher than 1. This is obviously due to the different populations, and therefore daily observed cases, of these municipalities. In addition, once again the  $R_t$  curves of the neighbouring pairs of municipalities resemble each other. See for example the curves of Alicante and Aigues which describe similar plateaus and peaks from May to mid September. This is, evidently, a consequence of the spatial dependence of rates since the observed cases in Aigues are not strong enough as to describe such a detailed temporal evolution.

In addition to enhanced (smoothed) spatio-temporal epidemiological indicators, as the case of the instantaneous reproduction number already shown, the spatio-temporal model proposed also allows performing deeper studies and developing surveillance tools of high epidemiological value. We show now some of these capabilities.

Figure 3 shows, for each region, a correlation plot for the coefficients of each function of the spline basis. The names in the rows and columns of the plot correspond to the day showing the peak of the corresponding spline function, in order to make temporal sense of the corresponding coefficients. It can be seen how, for both regions, all the coefficients previous to July show high correlations, regardless of the moment of the corresponding peak. On the contrary, this seems to change with the starting of July. This suggests that the geographical pattern of the pandemic was steady during the first wave of the pandemics but with the end of that wave, and also coinciding with the lift of the mobility restrictions by the Spanish government (active from March 14th to June 21st), the spatial pattern of the disease completely changed. In the case of CV this change was quite abrupt, the spatial patterns from July hardly show any correlation with the spatial patterns previous to that month, and milder in the case of CyL. These different patterns may be explained by the

large touristic sector of CV, whose coastline attracts millions of tourists each summer. This sector possibly attracted thousands of tourists coinciding with the starting of the summer and the lift of restrictions which could make its spatial pattern to change completely, in contrast to CyL where this change is milder.

Figure 3 shows some additional differences between CV and CyL spatial pattern evolutions. For example, in CV, we see from July a completely dynamic evolution of the pandemics since the spatial pattern corresponding to any spline function of this period hardly shows any correlation with the spatial pattern of the spline component corresponding to one month latter. Thus, the pandemics in CV during this period is moving around with no particular preference for any specific geographical location of this region, in contrast to the first phase of the pandemics when population was confined. In contrast, for CyL correlations show overlapping diagonal squares which points out a less haphazard evolution of the disease. Evidently, these plots could be further interpreted with the aid of some additional results. For example, Figure 5 of the accompanying supplementary material shows how the first wave of the pandemic in CyL was mainly urban while the second wave, at least its summer period, showed higher rates in the rural areas. This points out once again that tourism has possibly taken an important effect in the second pandemic wave also in this region, since rural zones receive most of the tourism in this inner zone of Spain, mainly during the summer period. Questions of this kind are not fully discussed in this paper for lack of space although they are, evidently, interesting results that can also be drawn from our model.

Figure 4 also illustrates some of the small areas analysis possibilities that our spatio-temporal model yields. As illustrated throughout this paper, both rates and  $R_t$ 's are the main focus of interest of most Covid-19 epidemiological analyses. These two indicators measure, respectively, the current state of the pandemics and its temporal evolution according to the latest data, a kind of derivative of the incidence curve. Therefore these two quantities are complementary indicators of the pandemics. Currently, the joint study of these two indicators has been proposed as a summary measure of the "risk" of the pandemics (<https://biocomsc.upc.edu/en/covid-19/Risk%20Diagrams>). The joint representation of these two indicators in a single plot has been proposed and used in an applied epidemiological context, but it has always been done for large areas (López Codina 2020), due to the statistical problems for dealing with these indicators when working with small areas. Nevertheless, our spatio-temporal model could be also used in this context, making it useful also for small areas problems, as illustrated in Figure 4.

The left-hand side of Figure 4 shows a joint plot of the incidence rate for the last 7 days, jointly with the  $R_t$  for each municipality in CV at the latest day of the period of study. Results could also be reproduced for previous days. Incidence rates for the last 7 days have been defined as 7 times the incidence rate for the latest day of study in order to represent the most updated information on the disease, according to the available data. Color cuts in this plot have been set as the different official risk levels for each of these indicators set by the Spanish government (Consejo Interterritorial, Sistema Nacional de Salud 2020), these are:  $\{10,25,75,125\}$  for the weekly incident rates and  $\{1,1.1,1.5,2\}$  for the  $R_t$ 's. Anyway, these cuts could be alternatively defined as a function of sample percentiles, for example, if this was found more convenient. Colors in Figure 4 have been chosen in order to represent different levels of increasing risk (higher as we move towards the upper-right side of the plot), varying from greens for the municipalities with lower rates and  $R_t$ 's and reds for the municipalities with high values for these two indicators. This plot shows how the highest rate corresponds to a municipality with around 800 incident cases per 100000 people and the highest  $R_t$  is above 2.5 for one municipality.

The right-hand side of Figure 4 shows the geographical mapping of the risks shown in the left-hand side plot of this same figure. Municipalities are colored in the right plot with the color (risk level) corresponding to the region where they lay in the left side plot. Interestingly, this choropleth map shows an evident spatial pattern, pointing out several regions of particularly high or low risks. This spatial pattern arises as a consequence of the spatio-temporal modelling strategy followed, since otherwise municipalities (mainly those less populated) would mostly show a noisy geographical pattern. This map could allow the epidemiological CV authority to focus its efforts on those municipalities that most require it.

## 4 Conclusions

This paper introduces small areas spatio-temporal analyses for Covid-19 epidemiological surveillance. Although the model introduced has been applied to Spanish data, in our opinion the methods developed could be perfectly applied to any other region with similar available data. In order to run our model only population and daily incident cases data are required, which does not seem a strong requirement.

We would like to mention an epidemiological limitation of the analysis we have carried out in this paper. It is widely known that Covid-19 incidence data for both epidemic waves in our case study, at least for Spain, are not comparable. The lack of diagnostic tests of the disease during the first pandemic wave, for example, makes the available data for that period to underestimate the height of that wave, making both waves uncomparable in absolute terms. Nevertheless, the

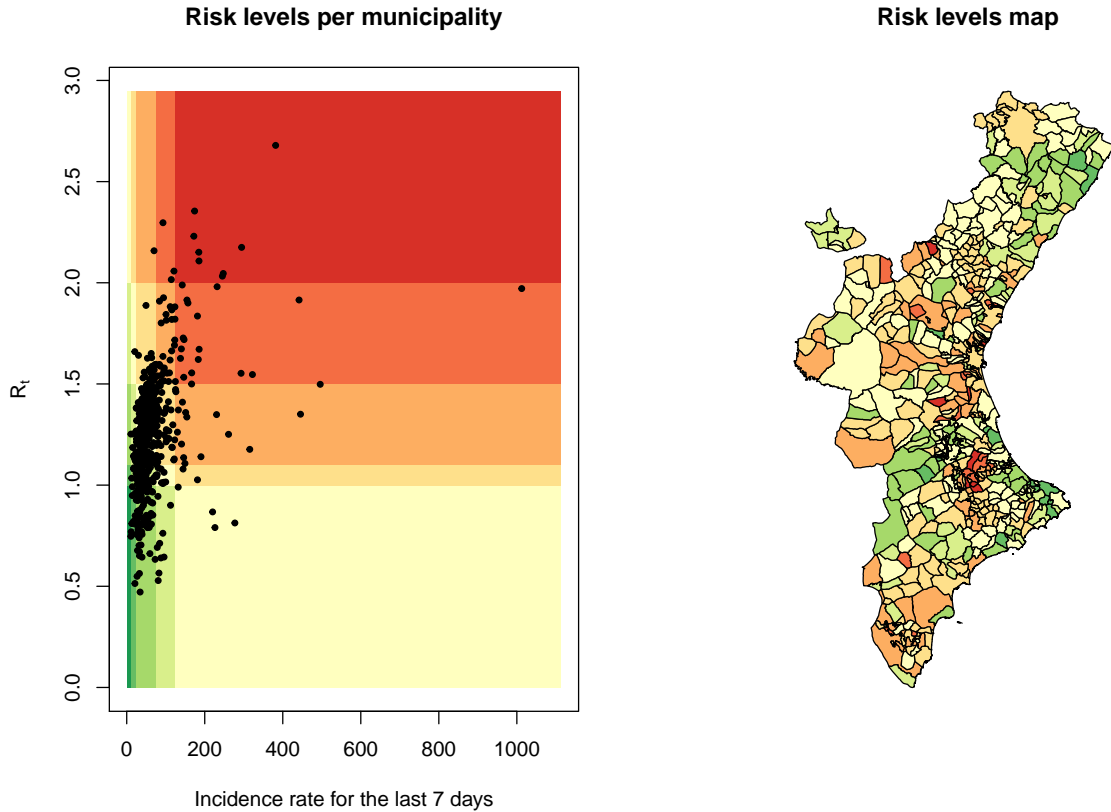


Figure 4: Risk levels according to smoothed weekly incidence rates and  $R_t$ 's and its geographical representation.

joint analysis of all the epidemic period of the disease (both waves) has allowed performing an overall analysis of the spatial distribution of the disease during all that period. In principle, the spatial distribution of the disease would not depend on the lack of diagnostic tests of the disease since this was something generalised for all CV and CyL. Anyway, direct comparisons of the strengths of the first and second epidemic waves should be, and have been, avoided.

One interesting aspect of our proposal is its computational performance. The dimensions of the data sets analysed for this paper are quite large, with  $120286 (= 223 \cdot 542)$  and  $55081 (= 223 \cdot 247)$  spatio-temporally correlated observations. Moreover, we have used a heteroscedastic spatio-temporal dependence structure for our analyses, which makes the underlying process more flexible but could also pose additional computational problems that we have been able to deal with. This has been possible due to the dimensionality reduction achieved by the use of the spline basis, which has reduced the number of spatial patterns to be fitted from 223 to just 17. This makes this fit of this model substantially faster than spatio-temporal models with one spatial process per time unit (Martinez-Beneito, López-Quílez, and Botella-Rocamora 2008). Nevertheless, the computing times required for fitting both data sets have been high (16.2 and 7.9 hours), respectively. Possibly, these computing times could be improved by using other MCMC sampling engines, such as Nimble or STAN. Nevertheless, for the usual case of being surveillance the main purpose of the study, in particular surveillance of the latest day of analysis, we would not need to consider such a long period of study. Most of the functions of natural B-spline bases have compact support so, for the latest day of study, increasing the period of analyses does not yield any improvement. The first splines in the basis will not take any effect on the final part of the period of study. In this case, reducing the days of analysis to the latest 56 days would reduce the spline basis to just 5 functions, reducing accordingly the computing time (for CV this reduces the computing time to just 1.16 hours), and producing the same fit for the latest day that if we considered a higher number of days for the analysis.

Most current Covid-19 epidemiological surveillance systems use incident rates for the last 7 or even 14 days. Using 14 days rates may seem justified as a proxy of disease prevalence, assuming that the disease (or its contagious period) lasts in average around 14 days to vanish. Similarly, 7 days rates seem also a reasonable option for removing the weekly cyclic character that data could supposedly show. Moreover, these two rates consider several days, increasing

therefore the number of observed cases used to compute each rate, what could alleviate the small areas problems that data could show and enable to calculate  $R_t$  estimates. Nevertheless, despite of these appealing features, epidemiologic surveillance with 7 or 14 days rates does not seem the best option. The aggregation of several days into intervals makes the corresponding rates to average the information of those time intervals, reducing therefore the novelty that surveillance epidemiological systems should supposedly have. Effective surveillance systems need data as actual and updated as possible and that feature is lost with the temporal aggregation of data. In this sense our model allows focusing our attention on the latest day of analysis, making Covid-19 surveillance more effective.

Undoubtedly, spatio-temporal analyses of the Covid-19 pandemics could provide important insight on the dynamics of the disease. As illustrated, these analyses have shown the effect of touristic activity on the diffusion and spatial distribution of the disease. Moreover, we have developed surveillance tools that allow to focus epidemiologists' attention wherever is required in order to contain the advance of the disease. Nevertheless, these analyses are useful only if small areas are used to perform statistical studies. If large areas of analysis were used instead, results and conclusions would be much less detailed and powerful, what would reduce the impact of those studies. Therefore, the development of small areas analysis tools seems necessary in order to increase the value of spatial epidemiological studies against Covid-19. This work is just a step in that direction.

## Bibliography

- Besag, Julian, Jeremy York, and Annie Mollié. 1991. "Bayesian Image Restoration, with Two Applications in Spatial Statistics." *Annals of the Institute of Statistical Mathematics* 43: 1–21. <https://doi.org/10.1007/BF00116466>.
- Centro Nacional de Epidemiología. Instituto de Salud Carlos III. 2020. November 1, 2020. <https://cnecovid.isciii.es/covid19/>.
- Consejo Interterritorial, Sistema Nacional de Salud. 2020. "Coordinated Response Actions for the Transmission Control of Covid-19 [in Spanish]." 2020. [https://www.lamoncloa.gob.es/serviciosdeprensa/notasprensa/sanidad14/Documents/2020/221020\\_ActuacionesrespuestaCOVID.pdf](https://www.lamoncloa.gob.es/serviciosdeprensa/notasprensa/sanidad14/Documents/2020/221020_ActuacionesrespuestaCOVID.pdf).
- Cori, Anne. 2020. *EpiEstim: Estimate Time Varying Reproduction Numbers from Epidemic Curves*. <https://CRAN.R-project.org/package=EpiEstim>.
- Cori, Anne, Neil M. Ferguson, Christophe Fraser, and Simon Cauchemez. 2013. "A New Framework and Software to Estimate Time-Varying Reproduction Numbers During Epidemics." *American Journal of Epidemiology* 178 (9): 1505–12. <https://doi.org/10.1093/aje/kwt133>.
- Fang, Yaqing, Yiting Nie, and Marshare Penny. 2020. "Transmission Dynamics of the COVID-19 Outbreak and Effectiveness of Government Interventions: A Data-Driven Analysis." *Journal of Medical Virology* 92 (6): 645–59. <https://doi.org/10.1002/jmv.25750>.
- Gelman, Andrew, Jon B Carlin, Hal S Stern, David B. Dunson, Aki Vehtari, and Donald B Rubin. 2014. *Bayesian Data Analysis*. 3rd ed. Boca Raton: Chapman & Hall/CRC.
- Han, Emeline, Melisa Mei Jin Tan, Eva Turk, Devi Sridhar, Gabriel M Leung, Kenji Shibuya, Nima Asgari, et al. 2020. "Lessons Learnt from Easing COVID-19 Restrictions: An Analysis of Countries and Regions in Asia Pacific and Europe." *The Lancet*, September. [https://doi.org/10.1016/s0140-6736\(20\)32007-9](https://doi.org/10.1016/s0140-6736(20)32007-9).
- Lawson, Andrew B. 2018. *Bayesian Disease Mapping: Hierarchical Modeling in Spatial Epidemiology (3rd Edition)*. CRC Press.
- Leroux, Brian G., Xingye Lei, and Norman Breslow. 1999. "Estimation of Disease Rates in Small Areas: A New Mixed Model for Spatial Dependence." In *Statistical Models in Epidemiology, the Environment and Clinical Trials*, edited by M E Halloran and D Berry. Berlin Heidelberg New York: Springer. [https://doi.org/10.1007/978-1-4612-1284-3\\_4](https://doi.org/10.1007/978-1-4612-1284-3_4).
- López Codina, Daniel. 2020. "Tools for Early Detection and Risk Assessment." In *COVID-19 & Response Strategy*, edited by ISGlobal. <https://www.isglobal.org/en/-/como-hacer-frente-a-los-nuevos-brotos-de-la-covid-19->.
- Martinez-Beneito, Miguel A., and Paloma Botella-Rocamora. 2019. *Disease Mapping from Foundations to Multidimensional Modelling*.
- Martinez-Beneito, Miguel A., Antonio López-Quílez, and Paloma Botella-Rocamora. 2008. "An Autoregressive Approach to Spatio-Temporal Disease Mapping." *Statistics in Medicine* 27: 2874–89.

- Milligan, Gregg N., and Alan D. T. Barrett. 2014. *Vaccinology: An Essential Guide*. John Wiley & Sons. <https://www.ebook.de/de/product/23507913/vaccinology.html>.
- Nishiura, Hiroshi, and Gerardo Chowell. 2009. “The Effective Reproduction Number as a Prelude to Statistical Estimation of Time-Dependent Epidemic Trends.” In *Mathematical and Statistical Estimation Approaches in Epidemiology*, 103–21. Springer Netherlands. [https://doi.org/10.1007/978-90-481-2313-1\\_5](https://doi.org/10.1007/978-90-481-2313-1_5).
- Nishiura, Hiroshi, Natalie M. Linton, and Andrei R. Akhmetzhanov. 2020. “Serial Interval of Novel Coronavirus (COVID-19) Infections.” *International Journal of Infectious Diseases* 93 (April): 284–86. <https://doi.org/10.1016/j.ijid.2020.02.060>.
- Rao, J N K. 2003. *Small Area Estimation*. John Wiley & Sons.
- Rue, Havard, and Leonhard Held. 2005. *Gaussian Markov Random Fields: Theory & Applications*. Chapman & Hall/CRC.
- Tebé, Cristian, Joan Valls, Pau Satorra, and Aurelio Tobías. 2020. “COVID19-World: A Shiny Application to Perform Comprehensive Country-Specific Data Visualization for SARS-CoV-2 Epidemic.” *BMC Medical Research Methodology* 20 (1). <https://doi.org/10.1186/s12874-020-01121-9>.
- Torres-Avilés, Francisco, and Miguel A. Martínez-Beneito. 2015. “STANOVA: A Smooth-ANOVA-Based Model for Spatio-Temporal Disease Mapping.” *Stochastic Environmental Research and Risk Assessment* 29 (1): 131–41. <https://doi.org/10.1007/s00477-014-0888-1>.
- Vergara-Hernández, Carlos, and Miguel A. Martínez-Beneito. 2020. “Pbugs.” September 29, 2020. <https://github.com/fisabio/pbugs>.
- Wilasang, Chaiwat, Chayanin Sararat, Natcha C Jitsuk, Noppamas Yolai, Panithee Thammawijaya, Prasert Auewarakul, and Charin Modchang. 2020. “Reduction in Effective Reproduction Number of COVID-19 Is Higher in Countries Employing Active Case Detection with Prompt Isolation.” *Journal of Travel Medicine* 27 (5). <https://doi.org/10.1093/jtm/taaa095>.